Characterization of Heat Generation in Aged and Non-Aged Batteries for Electric Vehicle and Hybrid Electric Vehicle Application

An Undergraduate Honors Thesis

Submitted to the Department of Mechanical Engineering

The Ohio State University

In Partial Fulfillment of the Requirements

for Graduation with Distinction in Mechanical Engineering

Cassandra Carr

Spring, 2014

Dr. Marcello Canova, Advisor

Abstract

With increasing demand for electric (EV) and hybrid electric (HEV) vehicles, a longer lifespan battery for vehicle application has become more desirable. The lifespan of these batteries are largely dependent on their type of usage in various environmental conditions, such as current demand, discharge and charging rates, and temperature. In addition, it is essential to monitor the heat generation produced in batteries to prevent the development of "hot spots" in battery packs, shortening their lifespan. This research addresses this important idea to characterize both electrical performance and heat generation by developing an experimental methodology for thermal and electrical characterization of Li-Ion battery cells used for EV and HEV application. A set of tests have been developed using an isothermal battery calorimeter to characterize heat generation of Aged and Non-Aged Li-Ion battery cells at various charge/discharge rates. The outcome of this research will be fundamental to understanding long term degradation phenomena on electrical and thermal outputs of cells, and develop models to characterize the heat generation and temperature variation in battery cells

Acknowledgements

I would first off like to thank Dr. Marcello Canova for being my advisor on this project. He introduced me to the project and has helped to guide me towards completion of the project, even with the multiple obstacles we have faced. With his extremely busy schedule, he still choose to meet with me on a regular basis and provided important feedback and direction in order to guide me towards successful completion of this project.

I would also like to thank Dr. Shrikant Nagpure for his guidance in the lab and feedback on this project. He helped with experimental design, gave valuable knowledge on coin cell fabrication and testing, and produced all of the coin cells used for the data in this study.

In addition, I would like to thank the Ohio State Center for Automotive Research for allowing me to do my research at its facilities.

Table of Contents

Abstract **2**

Acknowledgements **3**

Table of Contents **4**

List of Figures **5**

List of Tables **6**

Chapter 1: Introduction and State of the Art **7**

Chapter 2: Description of the Experimental Setup **10**
- 2.1 Principles of Calorimetry
- 2.2 The Isothermal Battery Calorimeter
- 2.3 Coin Cell Fabrication and Preliminary Characterization
- 2.4 Procedure: Heat Capacity Test
- 2.5 Procedure: Charge-Discharge Test

Chapter 3: Overview of Electro-Thermal Models of Li-Ion Batteries **21**
- 3.1 Modeling Overview
- 3.2 Electrical Models
- 3.3 Heat Generation Models
- 3.4 Thermal Dynamics

Chapter 4: Results and Discussion **26**
- 4.1 Case Study 1: Heat Capacity
- 4.2 Heat Capacity Test Error Analysis
- 4.3 Heat Capacity Test Results
- 4.4 Case Study 2: Discharge Test
- 4.5 Discharge Test Error Analysis
- 4.6 Heat Generation Comparison for Different C-Rates
- 4.7 Heat Generation Comparison for Aged and Non-Aged

Chapter 5: Conclusion and Recommendation for Future Work **45**
- 5.1 Conclusion
- 5.2 Recommendation for Future Work

References **46**

List of Figures

Figure 1: The Ragone Plot for various energy storage devices **8**
Figure 2: The IBC laboratory setup **11**
Figure 3: Diagram of calorimeter chamber main components **12**
Figure 4: Fabricated coin cell structure **13**
Figure 5: LABstar Glovebox **14**
Figure 6: The main screen of the IBC Interface **15**
Figure 7: The settings for the IBC Interface **15**
Figure 8: Interface for Heat Capacity Testing with the IBC **17**
Figure 9: Interface for Battery Cycling with the IBC **18**
Figure 10: General summary of battery modeling **21**
Figure 11: Static 0th Order Equivalent Circuit Model **22**
Figure 12: Dynamic 1st Order Equivalent Circuit Model **23**
Figure 13: Energy balance for discharge and charge **23**
Figure 14: Lumped thermal model diagram **24**
Figure 15: The amount heat added or removed from a coin cell for a one degree temperature step **26**
Figure 16: The measured and idea capacity of copper for different masses **28**
Figure 17: Raw data from heat generation test **30**
Figure 18: The current during the one hour rest at the beginning of the test **31**
Figure 19: The current error throughout the rest, charge and discharge portion of the discharge test **32**
Figure 20: The heat during the one hour rest at the beginning of the test with the average shown in green **33**
Figure 21: Emphasis on the time constant experienced by the calorimeter **34**
Figure 22: Close up of raw data for discharge and resting portion of test **35**
Figure 23: Electrical model of a battery **35**
Figure 24: Verification of Calorimetry Heat Generation Data **37**
Figure 25: Voltage comparison of different C-Rates during discharge of a C04 coin cell **38**
Figure 26: Heat generation comparison of different C-Rates during discharge of a C04 coin cell **38**
Figure 27: Energy balance of a battery for charging and discharging **39**
Figure 28: Efficiency during discharge of C04 coin cell for different C-Rates **40**
Figure 29: Efficiency during discharge of C04 coin cell for different C-Rates **41**
Figure 30: Comparison of heat generation for aged vs unaged cells at C/5 **42**
Figure 31: Comparison of heat generation for aged vs unaged cells at C/2 **42**
Figure 32: Comparison of Internal Resistance for Aged vs Unaged cells **43**
Figure 33: Comparison of Efficiency for Aged vs Unaged cells **43**
Figure 34: Heat generation of two cells fabricated from the same unaged battery **44**

List of Tables

Table 1: The measured and calculated capacity of copper for different masses **27**
Table 2: The results of the heat capacity tests for both aged and unaged cells **29**

Chapter 1: Introduction and State of the Art

With fossil fuel prices continually increasing and demand in the market for more eco-friendly products, electric and hybrid electric vehicles have become a growing sector in the automotive industry. Over the past few years, major automotive manufacturers have released over 50 hybrid and electric vehicles onto the market, with some models showing great promise and revenue. The Toyota Prius has made the list for "The Top Ten Best-Selling Passenger Cars" [1] and this past year the Tesla Model S was named "Motor Trend's Car of the Year" [2]. Both of these awards have provided great optimism for the further growth of the electric and hybrid vehicle industry. From 2010, hybrid and electric vehicles have gone from taking up 2.37% to 3.86% of the auto industry [3], and with these numbers expecting to rise; automakers are becoming more interested in investing into the market.

However, it is essential to not only look at the trends in electric vehicles as a whole but also the electrical powertrains that "fuel" them. Currently, lithium ion batteries have been the choice of the industry due to their high energy density and long life cycle [4]. As seen in Figure 1, Li-Ion Batteries cover a wide range of specific energy and specific power compared to other battery types.

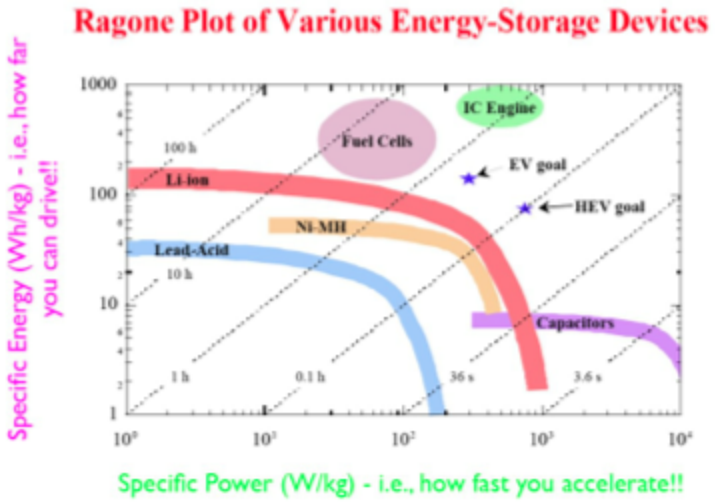

Figure 1: The Ragone Plot for various energy storage devices [5]

One of the key limiting factors to lithium ion batteries is the narrow window for proper operating conditions (approximately 0 to 65°C) in order to maximize efficiency, lifespan, and safety [6]. In addition, as batteries become more widely used for vehicle application, a more detailed evaluation of how batteries behave throughout their lifespan is necessary. Unfortunately, with both of these items, a proper solution is difficult. Like all batteries, lithium ion cells are highly exothermic during charging and discharging, but the complicated system that makes up the battery is difficult to study because of the various processes and interactions occurring at once. Thus, as one looks into aging and thermal management, processes cannot be studied independently and conclusions are hard to make [7].

Currently, characterization of these systems has been studied using various methods such as Electrochemical Impedance Spectroscopy (EIS), Electrical Testing, and Calorimetry Testing. During EIS testing, a frequency domain analysis is used to develop a Nyquist plot of the cell impedance, which can be used to determine cell

energy storage properties [8]. However, interpretation of impedance data can be challenging. In Electrical Testing, current cycling is used, however, most electrical properties are reliant on temperature, giving an incomplete picture. With Calorimetry Testing, one is able to develop plots of the heat generation developed during different battery cell operations at various parameters, such as temperature. The calorimeter records the amount of heat generations during these various processes and this data can be studied to conclude certain trends. Overall, various testing has concluded that material parameters, storage conditions, and cycling conditions all have an impact on battery lifespan and performance. High and low state of charge can shorten life, and operating at high and low temperatures can also have a negative impact [7].

During this study, the method of calorimetry will be used on coin cells harvested from larger batteries used for electric vehicle applications. Coin cells from aged and unaged cathode material will be tested for Heat Capacity and heat generation will be measured during discharge of these cells at different capacity rates. This experimental data will be plotted and plots will be compared between aged and unaged cells in order to provide further insight on the changes in heat generation brought about from an aging battery. This study will not only look at these trends, but will develop a methodology for characterizing the heat generation of a battery cell throughout its lifespan.

Chapter 2: Description of the Experimental Setup

2.1 Principles of Calorimetry

Calorimetry is defined as the study of parameter changes by quantifying the heat associated with that change [9]. During this study, calorimetry was used to characterize the heat loss associated with various charge and discharge profiles on a battery used for vehicular applications.

In studying calorimetry, a calorimeter is used to measure the heat formation. Although a calorimeter can be as simple as a thermometer in a bath of water surrounding an area of study, two specific types of calorimeters were compared for this study: isothermal and adiabatic.

An adiabatic calorimeter runs in an adiabatic environment, and as the reaction generates heat, the temperature of the sample is increased. However, no adiabatic calorimeter is ideal and there is always some loss of heat from the measured chamber. This error must be accounted for by a mathematical correction factor [10].

In contrast, an isothermal battery calorimeter measures heat released under isothermal conditions. As heat is generated during the reaction, it is removed and measured in order to keep the temperature of the sample constant. However, some error can be created from the increased capacity of the system due to the surrounding battery chamber. It has also been shown that Isothermal Battery Calorimeters have a greater sensitivity than adiabatic calorimeters [11].

2.2 The Isothermal Battery Calorimeter

The instrument used in this study was an isothermal battery calorimeter, or IBC, and was selected because heat generation data could be directly measured for different cycling properties and set temperature conditions. Heat generation data collected from the IBC was then used to evaluate the performance of a battery with respect to aging, establish battery heat generation trends, and also measure battery efficiency with time. In addition, the heat capacity of the battery, a key factor in battery thermal management design calculations, could be measured [12]. The IBC used in this study can be seen in Figure 2.

Figure 2: The IBC laboratory setup

From the IBC, four parameters (voltage, current, temperature, and heat) were collected and recorded with time for all tests [13]. Current, voltage, and temperature were parameters set by the user, while the changes in heat were recorded as result of the input parameters. The inner chamber of the calorimeter can be seen in Figure 3. A current lead and voltage sensor are used to control the electrical inputs, while the

heat flux sensor and thermocouple control the peltier junction. The peltier junction, in return, adds or removes heat to keep the temperature in the chamber constant. It is important to note that plate between the coin cell and the heat flux sensor creates a time constant in the heat data.

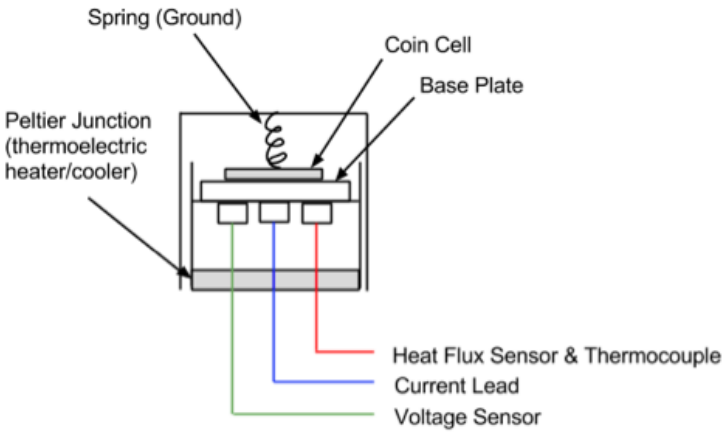

Figure 3: Diagram of calorimeter chamber main components.

The IBC was utilized for two tests in this study, heat capacity and multi-rate capacity. During the heat capacity test, heat generation data was recorded for a one-degree temperature step, which could then be used to determine the heat capacity of the coin cell being tested. For the multi-rate capacity test, heat generation was recorded for different current profiles. The current profile consisted of charging the cell from the minimum voltage to the maximum voltage limit at low capacity rates, followed by discharging the cell from the maximum voltage to the minimum voltage limit at higher capacity rates. The charging and discharging current was held constant throughout the test, and the test was ran for a range of capacity values.

The heat, current, and voltage data taken from the IBC during the multi-rate

capacity test could then be used to determine important parameters of the battery cell being tested such as efficiency, internal resistance, and general heat generation trends. This study looks at how to use calorimetry data from the tests described to successfully determine these parameters and how to use the results to compare aged and unaged battery cells.

2.3 Coin Cell Fabrication and Preliminary Characterization

The battery measured by the IBC in this study was a typical coin cell (CR2032). In order to measure larger battery packs used for vehicular application, coin cell half-cells were fabricated from unaged and aged A123 battery packs. Battery packs were aged using a low state of charge range (0-10%) and low C-Rate (4C) at a temperature of 55°C.

The fabricated coin cells consisted of a lithium reference electrode, a cathode or anode, a spacer, a spring, and coin cell casings. The structure of the coin cell can be seen in Figure 4.

Figure 4: Fabricated coin cell structure

All components of the fabricated coin cell were assembled in a LABstar

Glovebox, seen in Figure 5, which provides an Argon environment, primarily free of oxygen and water.

Figure 5: LABstar Glovebox

Once all components are assembled in the order shown in Figure 4, a crimping mechanism is used to seal the cell. The cell is then left to settle for 12 hours. Following this time frame, preliminary cycles are performed on the cell using a potentiostat to allow formation reactions to occur and let the system stabilize. The cell is initially cycled at C/50, followed by cycles at C/20 until the cell reaches a steady state [8].

2.4 IBC Software Overview

After coin cells completed the formation cycle, they were tested in the IBC. In order to interface with the IBC, a software program was used to input tests parameters. Figure 6 shows the main screen for the IBC software interface. Two headers to note are “Experiment Type” and “Tools.” “Experiment Type” directs the user to start Battery Cycle and Heat Capacity Tests, described in Sections 2.5 and 2.6. “Tools” directs the user the settings menu for the IBC. The settings menu can be seen in Figure 7.

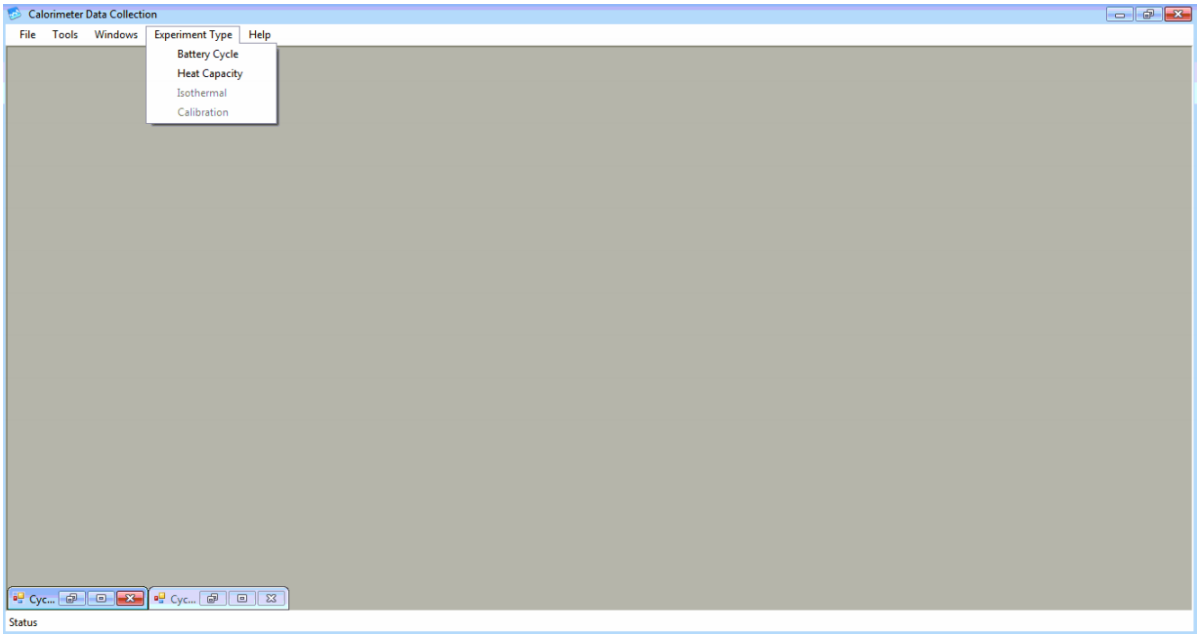

Figure 6: The main screen of the IBC Interface

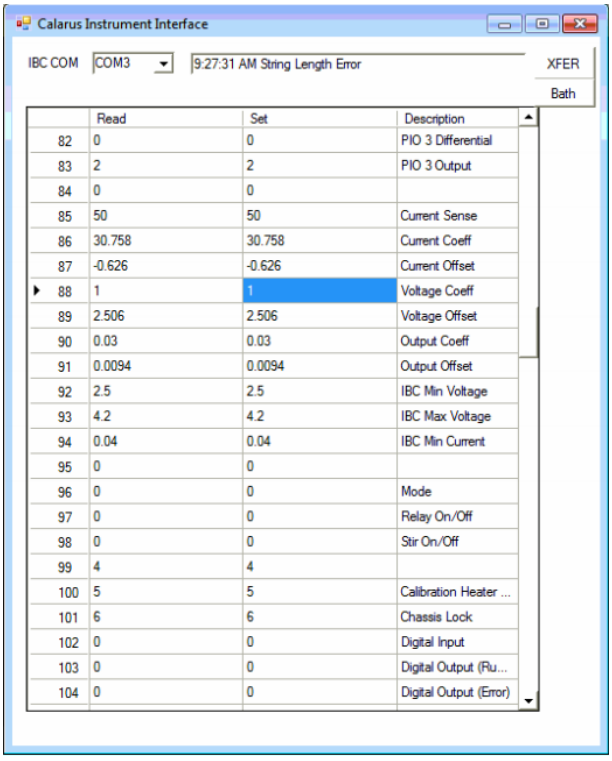

	Read	Set	Description
82	0	0	PIO 3 Differential
83	2	2	PIO 3 Output
84	0	0	
85	50	50	Current Sense
86	30.758	30.758	Current Coeff
87	-0.626	-0.626	Current Offset
88	1	1	Voltage Coeff
89	2.506	2.506	Voltage Offset
90	0.03	0.03	Output Coeff
91	0.0094	0.0094	Output Offset
92	2.5	2.5	IBC Min Voltage
93	4.2	4.2	IBC Max Voltage
94	0.04	0.04	IBC Min Current
95	0	0	
96	0	0	Mode
97	0	0	Relay On/Off
98	0	0	Stir On/Off
99	4	4	
100	5	5	Calibration Heater ...
101	6	6	Chassis Lock
102	0	0	Digital Input
103	0	0	Digital Output (Ru...
104	0	0	Digital Output (Error)

Figure 7: The settings for the IBC Interface

The settings menu allows the user to adjust various parameters that control

how the IBC collects data, such as the PID controller gain and integral settings. It also allows the user input which COM port the IBC is connected to. Before being able to collect data, the proper COM port must be selected. In addition, before each test the "Current Offset" setting was adjusted zero the current.

2.5 Procedure: Heat Capacity Test

A battery's heat capacity, defined as the amount of heat needed to raise the battery temperature one degree, is an important parameter needed for calculations characterizing battery behavior. In this study, the heat capacity of each tested coin cell was determined. The amount of heat added to the coin cell in order to raise it one degree Celsius and the amount of heat released by the coin cell in order for it to reduce one degree Celsius was recorded.

The IBC was used to gather this data, necessary for calculating the heat capacity of the coin cell tested. The software interface for running the heat capacity test with the IBC can be seen in Figure 8.

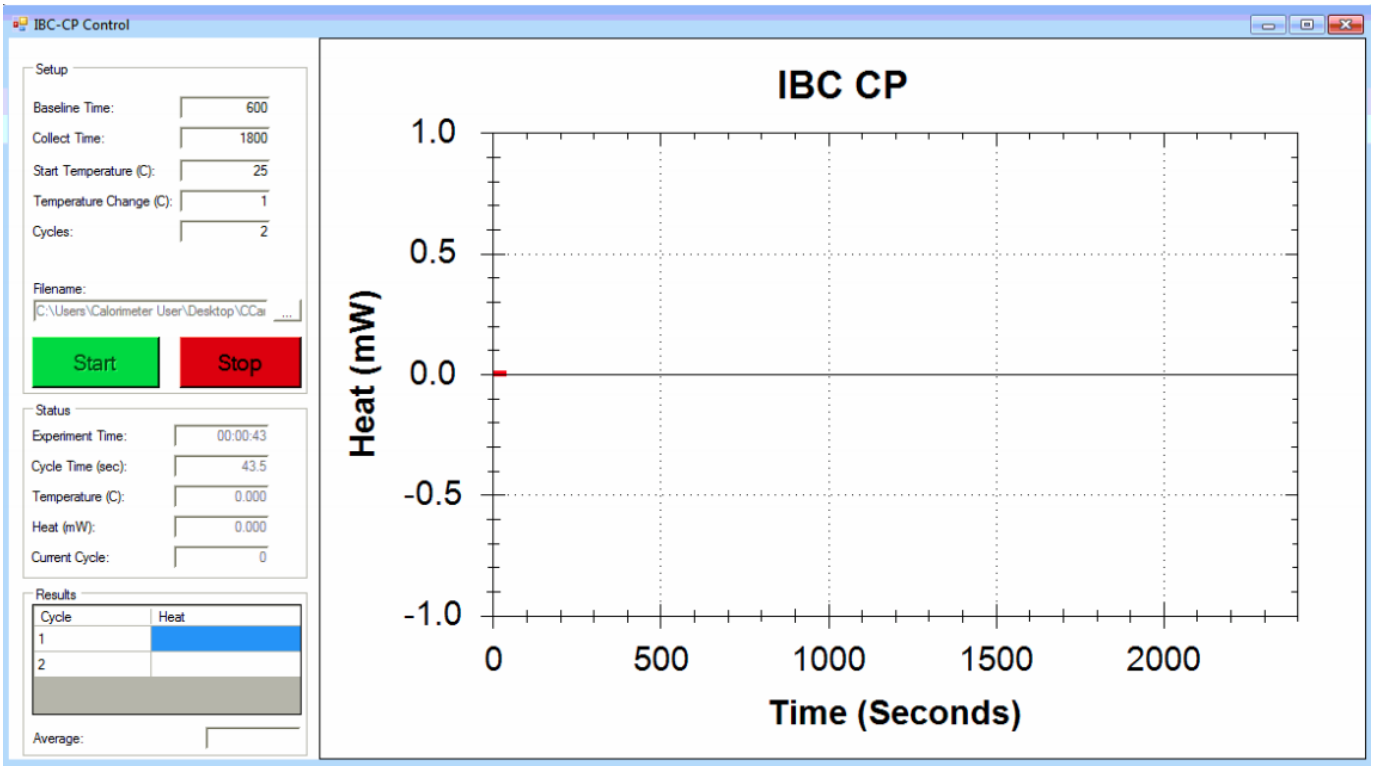

Figure 8: Interface for Heat Capacity Testing with the IBC

The various input parameters are seen in Figure 8 under Setup. "Baseline Time" refers to the wait time before the test begins in order to let the temperature equilibrate. "Collect Time" is the time data is collected from the start of the temperature step. "Start Temperature" is the baseline temperature. "Temperature Change" is the temperature step above the baseline temperature.

Once the input parameters are entered by the user, the filename can be selected and the "Start" button is pressed to begin the test. When the test is complete, the IBC software will automatically calculate the heat capacity in J/°C. The raw data is saved in the file directory indicated with the filename. For each cell, three tests were ran with the same parameters and the heat capacity value was determined from the average.

2.6 Procedure: Charge-Discharge Test

Understanding heat generation behavior during charging and discharge of a battery is key to developing better thermal management systems for batteries. In this study, charge-discharge tests were performed using the IBC and the heat generation data was collected for both aged and unaged fabricated coin cells. The software interface for battery cycling can be seen in Figure 9.

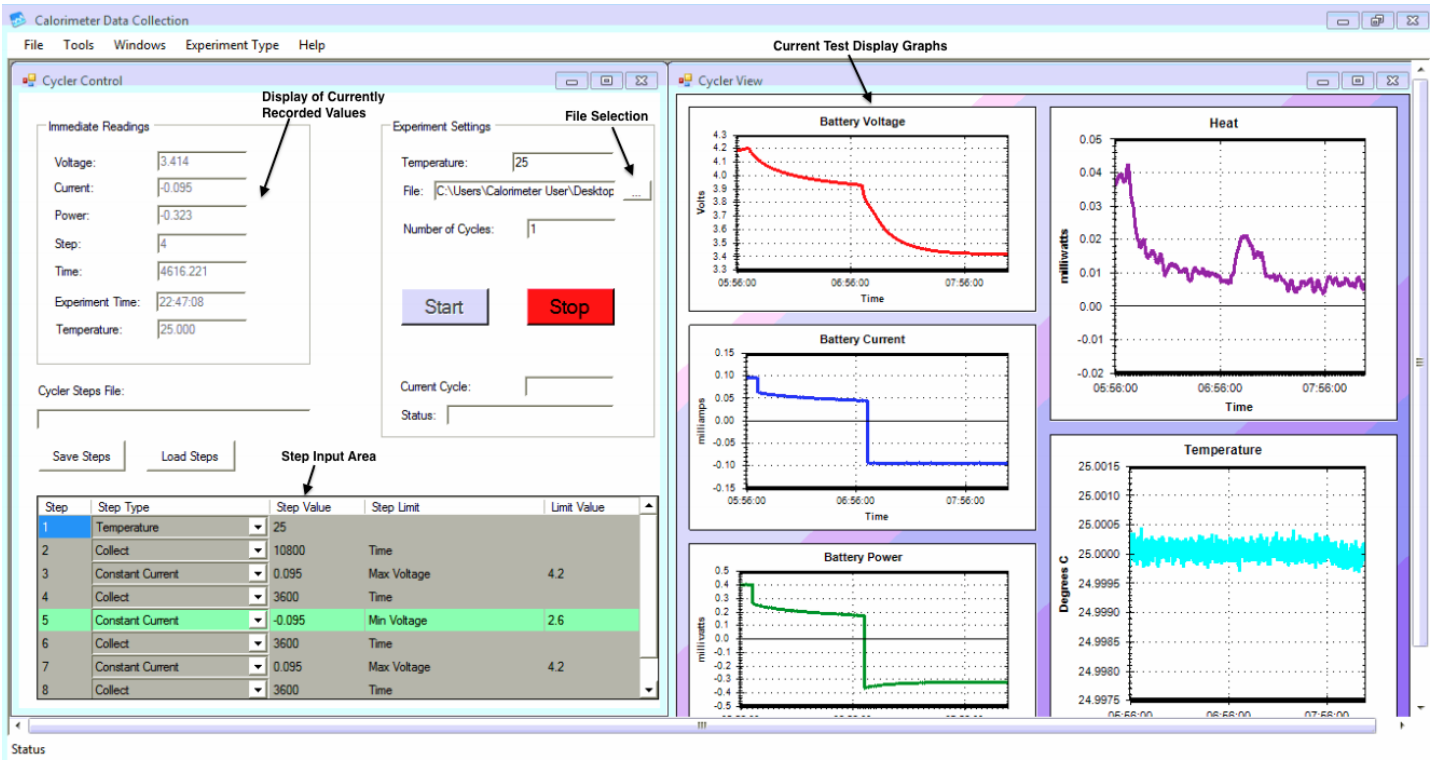

Figure 9: Interface for Battery Cycling with the IBC

Tests were set up by inputting the testing steps into the step input area. Steps can be defined as Temperature, Collect, Constant Current, or Constant Voltage. Temperature is typically input first in order to define the temperature the test is to be ran at. Collect represents a time when no current is imposed, but data is still collected (also referred to at “rest time”). Constant Current and Constant Voltage are

steps where a constant current and constant voltage are imposed on the cell, respectively.

The “Step Value” is associated with each inputted “Step.” For Temperature, it is the temperature in degrees Celsius. For Collect, it is the time in seconds. For Constant Current, it is the imposed current in milliamps, a negative value represents discharging and a positive value represents charging. For Constant Voltage, it is the imposed voltage in volts.

The “Step Unit” will automatically populate based on the “Step Value” entered. The “Step Unit” represents the limiting factor of the step (ie: if you are running a constant current discharge, the limiting factor will be maximum voltage).

For Constant Current and Constant Voltage Steps, the “Unit Value” will need to be input by the user. This is the value of the “Step Unit,” or what is the limiting factor of the step. For example, take note of the green highlighted values of Figure 9, for this step there is constant current discharging of -0.095mA to a Minimum Voltage value of 2.6V.

Once all of the steps are selected by the user, a file location and filename must be selected so the software can save the data collected (labeled in Figure 9). The user can then enter the number of cycles this test is to be run for. After all of the information in inserted, the user can press the “Start” button and the test will begin. Graphs on the right hand side of the screen will show the data collected and real time values of the data can be seen under “Immediate Readings.”

The test can be stopped at any time using the red “Stop” button. Once the test

is completed, the “Stop” button will appear grey. The data can be found in the file specified at the beginning of the test. In order to analyze the data, an extension can be added to the end of the file name of either “.txt” or “.csv” format. The file structure consists of columns of data in the following order: Experiment Time (s), Step Time (s), Temperature (C), Heat (mW), Voltage (V), Current (mA), and Mode.

Chapter 3: Overview of Electro-Thermal Models of Li-Ion Batteries

3.1. Modeling Overview

Modeling the performance of batteries is a very important part of R&D and other related activities of battery development, including the design of battery packs, system integration, and thermal management. With battery modeling, sets of equations can be formed to describe the performance and dynamic response of the battery. In this study, electrical and heat generation models were lumped to form a thermal dynamic model in order to analyze the data collected during calorimetry testing.

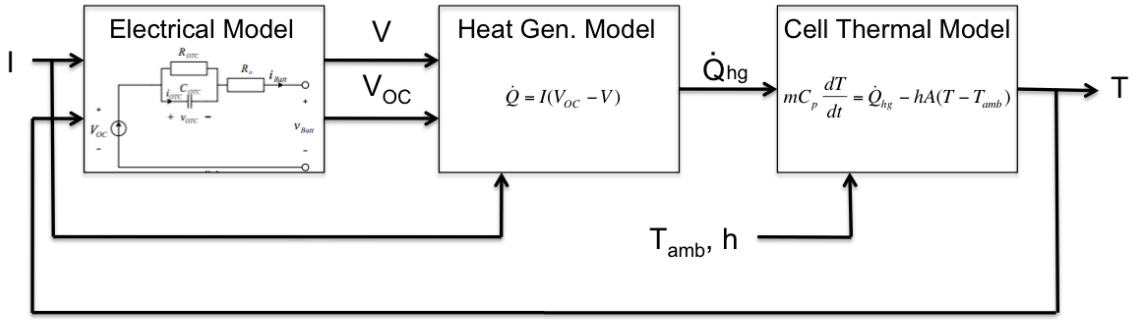

Figure 10: General summary of battery modeling [14,15]

Figure 10 shows a summary of the three models used in general battery models and their relationship to one another.

3.2. Electrical Models

Electrical models are used in battery modeling to relate the internal resistance and open circuit voltage to the voltage and current data collected from a battery during testing. In order to find the open circuit voltage of a battery at any point during charging and discharging, a curve relating open circuit voltage (OCV) to

the state of charge (SOC) of a battery must be developed. For modeling purposes, the OCV of a battery is defined as the voltage of the battery when charged or discharged at one-twentieth of the capacity (C/20) of the battery. The SOC during the charging or discharging process is calculated using Equation 1.

$$SOC = SOC_o - \frac{1}{C_{nom}} \int Idt \quad (1)$$

where C_{nom} is the Capacity of the cell

In this study, two OCV vs SOC curves were established from the minimum to the maximum battery voltage range. One was developed for charging at C/20 and the other for discharging at C/20. The average of the two curves was used for analysis, and was referenced in electrical models to find the OCV at any SOC.

Both static and dynamic models have been established to relate voltage and current to battery resistance and open circuit voltage at various SOC. The static model is seen in Figure 11 and defined by Equation 2.

$$V(t) = V_{oc} - R_o I(t) \quad (2)$$

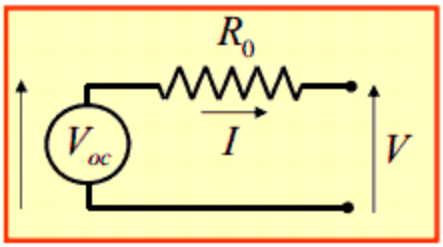

Figure 11: Static 0th Order Equivalent Circuit Model

The dynamic model is similar, but includes an RC loop which models a dynamic response with a time constant equal to RC. It is more accurate than the static model, but contains more parameters. The dynamic model is seen in Figure 12 and is defined

by Equation 3.

$$V(t) = V_{oc} - R_o I(t) - V_1(t) \quad (3)$$

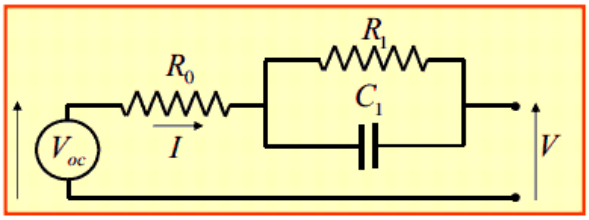

Figure 12: Dynamic 1st Order Equivalent Circuit Model

3.3. Heat Generation Models

When thinking of a battery as an energy converter, a simple energy balance can be used to relate heat to electrical energy. Figure 13 shows the energy balance for discharging and charging of a battery.

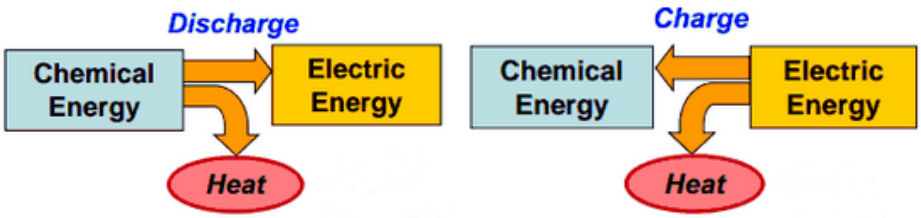

Figure 13: Energy balance for discharge and charge

When discharging a battery, chemical energy is converted to electrical energy and some of the energy is lost to heat. In charging, electrical energy is converted to chemical energy and some of the energy is lost to heat.

Taking this into account, heat generation can be directly related to efficiency. For the discharging case, Equations 4-6 can be established.

$$P = IV \quad (4)$$

$$P_{ideal} = IV_{oc} \quad (5)$$

$$\eta_{discharge} = \frac{P}{P_{ideal}} = \frac{V}{V_{oc}} \quad (6)$$

Similarly, for the charging case, Equation 8 is developed.

$$\eta_{charge} = \frac{P_{ideal}}{P} = \frac{V_{oc}}{V} \quad (7)$$

Using the energy balance, Equation 8 is used to relate P_{ideal} to heat generation.

$$P_{ideal} = P + \dot{Q} \quad (8)$$

With Equation 8, Equations 6 and 7 can then become:

$$\eta_{discharge} = \frac{P}{P+\dot{Q}} \quad (9)$$

$$\eta_{charge} = \frac{P+\dot{Q}}{P} \quad (10)$$

In summary, heat generation is related to voltage, open circuit voltage, and current, as seen in Equation 12.

$$\dot{Q} = P_{ideal} - P = I(V_{oc} - V) \quad (11)$$

3.4. Thermal Dynamics

Lumped parameter thermal models can be used to approximate the thermal behavior of a system, and can be seen in Figure 14. The heat generation model utilizes Equation 12 to take input parameters I(t), V(t), and $V_{oc}(t)$ and output the theoretical battery heat generation. This output is then used as an input to the lumped thermal model to find the temperature of the cell.

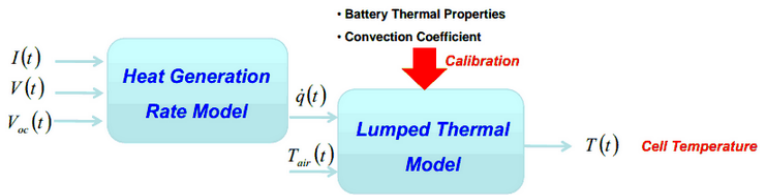

Figure 14: Lumped thermal model diagram

The lumped thermal model utilizes basic concepts of heat transfer due to convection as seen in Equation 12, where "hA" is the heat transfer per unit cell and "T_∞" is the temperature of air.

$$\dot{Q}_{heat\ transfer} = hA(T - T_\infty) \quad (12) \ [16]$$

Equation 13 shows how the lumped thermal model relates to the heat generation model, where "mc" refers to the heat capacity of the cell.

$$mc\frac{dT}{dt} = \dot{Q}_{gen} - \dot{Q}_{heat\ transfer} = I(V_{oc} - V) - hA(T - T_\infty) \quad (13)$$

The lumped thermal and heat generation models are key to interpreting data from the calorimeter. In calorimetry, output parameters consist of I(t), V(t), T(t), and Q(t). With I(t), the known capacity of the cell and an OCV vs SOC curve is able to be established. Thus, $V_{oc}(t)$ can be determined. With this information, a theoretical value for Q(t) can be calculated with the heat generation model and compared to the output of the calorimeter. Also, since the isothermal calorimeter keeps temperature constant during testing, Q_{gen} is found to be equal to $Q_{heat\ transfer}$. This relationship can be used to find useful parameters such as the heat transfer per unit cell (hA), however this is not performed in this study. Internal resistance of the battery can also be established through the relationships found in the electrical model, where the heat generation is approximately equal to the power generated by the battery. Overall, modeling allows for a more refined approach in the interpretation of calorimetry data.

Chapter 4: Results and Discussion

4.1 Case Study 1: Heat Capacity

Heat Capacity tests were performed for aged and unaged fabricated cathode coin cells. As discussed in Section 3.4, an important factor in utilizing the thermal model for batteries is the specific heat capacity of the battery. Equation 13 shows where this is significant. For heat capacity tests taken with the calorimeter, Figure 15 is produced from temperature and heat data collected.

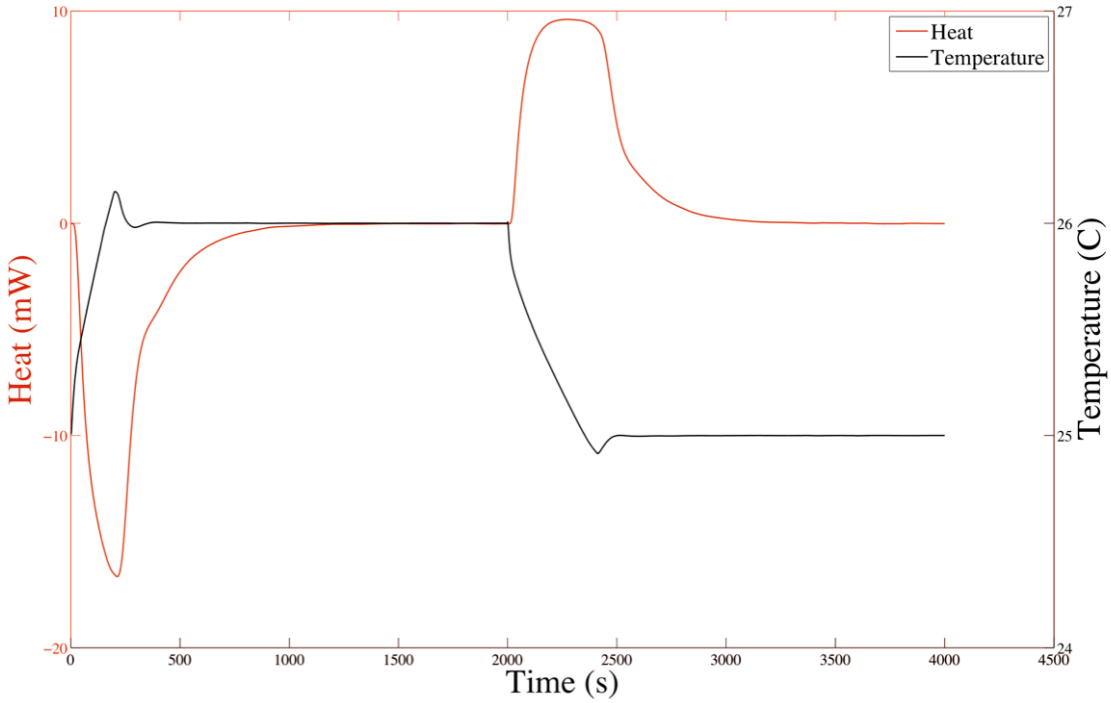

Figure 15: The amount heat added or removed from a coin cell for a one degree temperature step

During testing, heat generation is recorded for a one-degree temperature step. The quantity of heat added during the one degree temperature rise is calculated by taking the integral of the initial heat curve. For the one degree temperature

reduction, the quantity of heat removed is calculated in the same manner by taking the integral of the second heat curve. The average of the two heat calculations is then used as the heat quantity "Q" used in Equation 14. Along with the calculated heat, the mass of the cell and the temperature step (one degree celsius) are needed to calculated the specific heat capacity of the cell (C_p).

$$C_p = \frac{Q}{\Delta T * Mass} \quad (14)$$

4.2 Heat Capacity Test Error Analysis

In order to ensure proper heat capacity readings from the calorimeter, an error analysis was performed. A method for determining systematic error was developed before determining the heat capacity of the coin cells being tested in this study. It is important to note that the value of heat (Q) used in Equation 14 is the total heat to raise not only the coin cell one degree celsius, but the surrounding calorimeter chamber as well. The capacity of the calorimeter chamber acts as a blank offset and a method for accounting for this offset was developed.

Coins of various masses were made of solid copper and the heat capacity of each was measured and compared to the known value of copper. Four different masses of copper were tested in the calorimeter and the measured capacity of the copper was calculated. This was then compared to the known capacity of copper, calculated by multiplying the known specific heat capacity of copper (0.385 J/°C-g) to the mass of the tested coin. The results can be seen in Table 1.

Mass Cu (g)	**$C_{measured}$ (J/°C)**	**C_{true} (J/°C)**
8.4	5.8582	3.234

5.44	4.43	2.0944
3.69	3.5724	1.42065
2.57	2.9836	0.98945

Table 1: The measured and calculated capacity of copper for different masses

The measured heat capacity and true heat capacity of copper were then plotted for the different masses and compared. This can be seen in Figure 16.

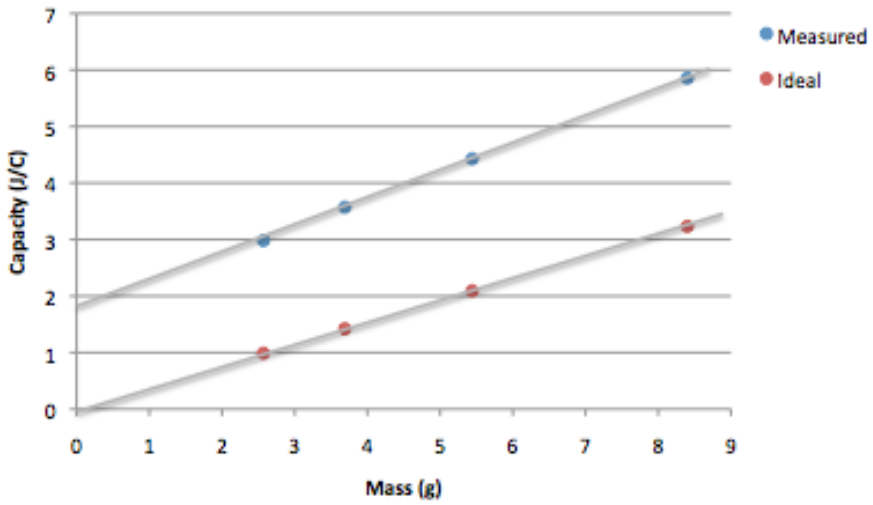

Figure 16: The measured and ideal (true) capacity of copper for different masses

The difference between the measured and ideal heat capacity of each copper mass was used to develop an error model for the calorimeter. This model was found to be linear with a slope accounting for a proportionality error and a y-intercept accounting for the blank offset. The error model was calculated as $y=0.1062(x)+1.7427$, where x is the mass of the cell and y is the capacity in J/°C.

4.3 Heat Capacity Test Results

Table 2 shows the heat capacity results of tests done on three different types of fabricated coin cells. The values were found to be relatively consistent, however, no

significant conclusions can be made until further testing is performed. The specific heat capacity was calculated using Equation 15.

$$C_p = \frac{0.1062(C_{measured})+1.7427}{mass} \qquad (15)$$

	Li-Li	C11 Unaged Anode	C04 Aged Cathode
Measurement 1 (J/C)	4.634	4.421	3.795
Measurement 2 (J/C)	4.633	4.427	4.445
Measurement 3 (J/C)	4.653	4.426	4.436
Measurement 4 (J/C)			4.45
Average Measurement (J/C)	4.6400	4.4247	4.2815
Mass (g)	4.4190	3.4870	3.56
Measured Heat Capacity (J/C)	4.64	4.42	4.28
Corrected Heat Capaicty (J/C)	2.43	2.31	2.16
Specific Heat Capacity (J/C*g)	0.55	0.66	0.61

Table 2: The results of the heat capacity tests for both aged and unaged cells

Overall, the heat capacity of fabricated coin cells was able to be calculated with the IBC and a proper methodology was established as outlined.

4.4 Case Study 2: Discharge Test

A heat generation comparison was performed with the calorimeter on an aged cathode C04 fabricated coin cell and unaged cathode C11 fabricated coin cell. A comparison was established for different capacity rates (C-Rates) of the C04 cell. In addition, the C04 aged cell and the C11 unaged cell were compared. The following testing procedure was used for each test performed:

1) Charging at C/20 to a maximum voltage of 4.2V

2) Discharging at a designated discharge rate of C/5, C/2, or 1C to a minimum voltage of 2.5 V

3) Rest for 8 hours

Figure 17 shows this test in full. This test was ran on aged and unaged fabricated cathode half cell coin cells at discharge rates of C/5, C/2, and 1C.

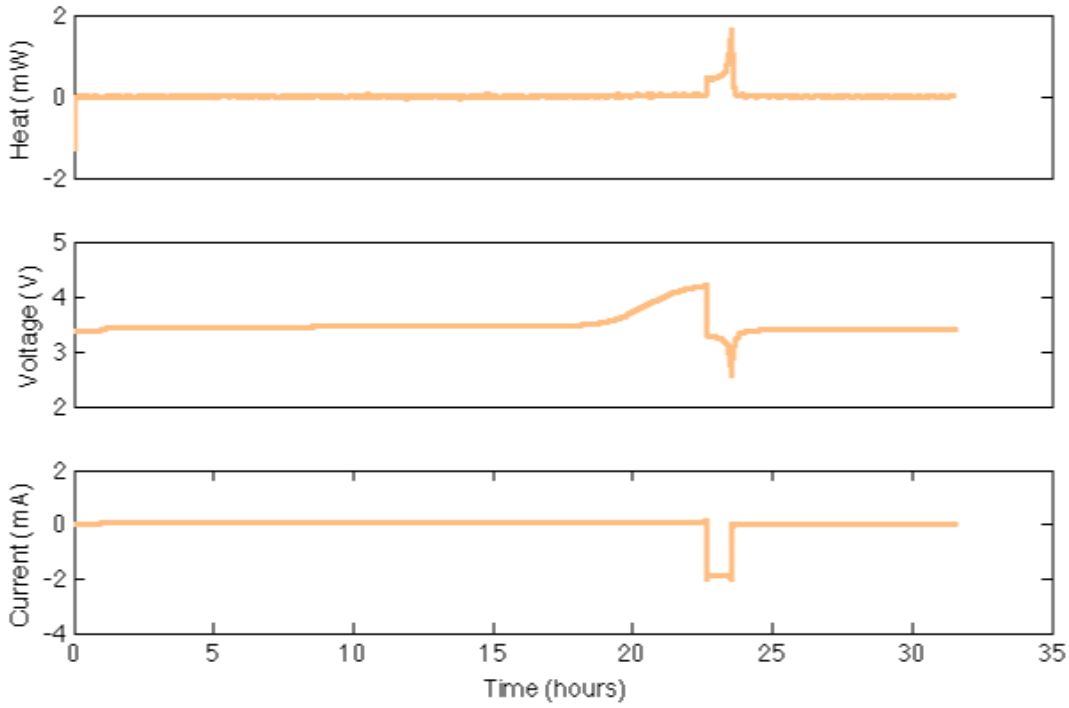

Figure 17: Raw data from heat generation test

The initial C/20 charge was performed at the beginning of each test to ensure that the state of charge at the beginning of the discharging portion was consistent for all tests. However, only the discharge and resting portion of each test was used for comparison.

4.5 Discharge Test Error Analysis

An error analysis was performed for different parameters taken during the discharge test. Error found in the current and heat, in addition to the system's dynamic response, were studied to see the effects on the results.

When studying the effects of error on the current, there was a random and systematic error identified. The systematic error was first removed by adjusting for an offset in the current. Figure 18 shows the first hour of testing, where there was a resting portion (current was set to zero). The average value of the current during this testing period was determined and subtracted from all following values in order to account for this offset.

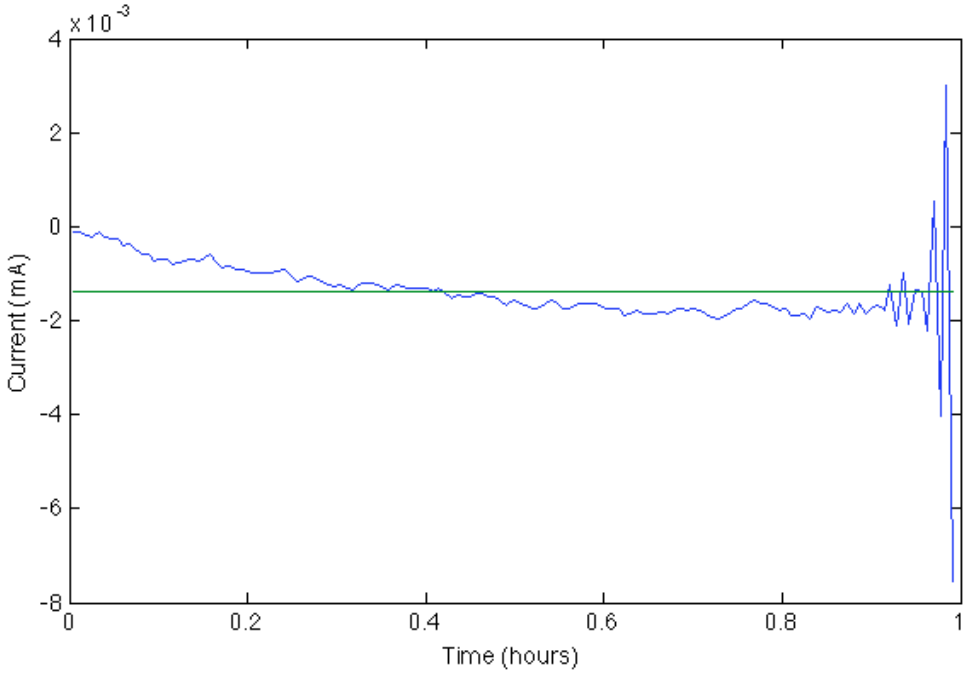

Figure 18: The current during the one hour rest at the beginning of the test with the average shown in green

After the current offset was accounted for, noise (or random error) was observed. Figure 19 shows the noise in the current during the first three steps in testing: 1 hour rest where current was set to zero, charging at C/20, and discharging at C/5 (or C/2, 1C). In order to develop this plot (Figure 19), the current value set by the user was subtracted from the reading generated by the calorimeter.

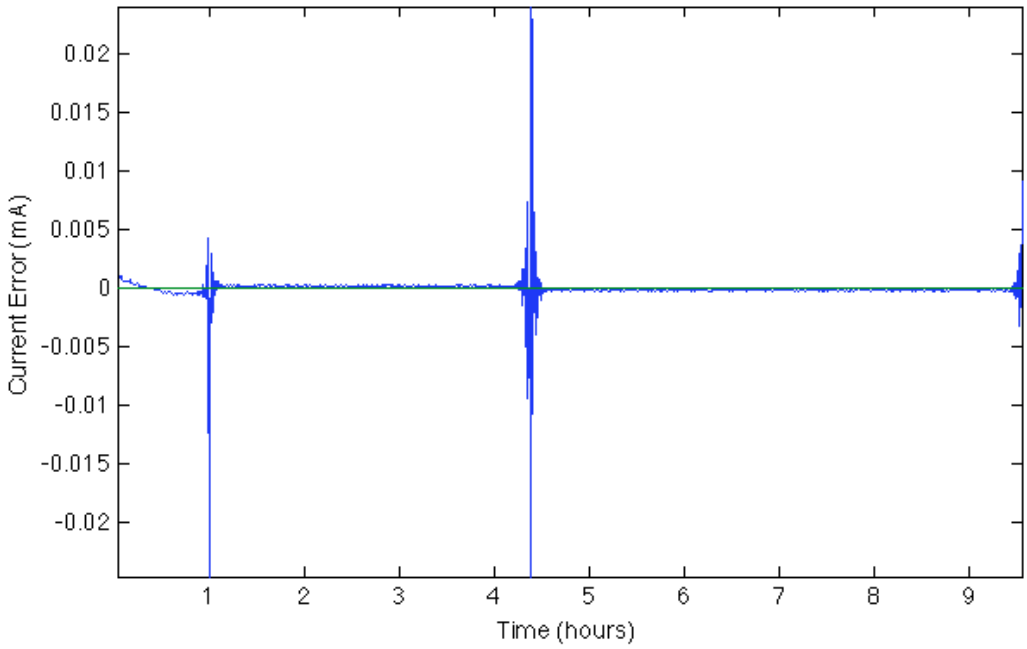

Figure 19: The current error throughout the rest, charge and discharge portion of the discharge test

As seen in Figure 19, the error in the current was very minimal, with the majority of the error staying with in a +/-0.01mA window. Considering C/5, or 0.38mA, was the minimum current of interest, the error can be calculated to be around 2.6%, an acceptable value. It is also important to note that the larger error in the current was found to be around transient conditions (where current was given a step input). These transient conditions were outside this study's area of interest (in this study primarily constant conditions were studied).

In addition to the error in the current, the error in the heat was observed. Similar to the current, an offset and noise could be identified. These two types of error can be seen in Figure 20.

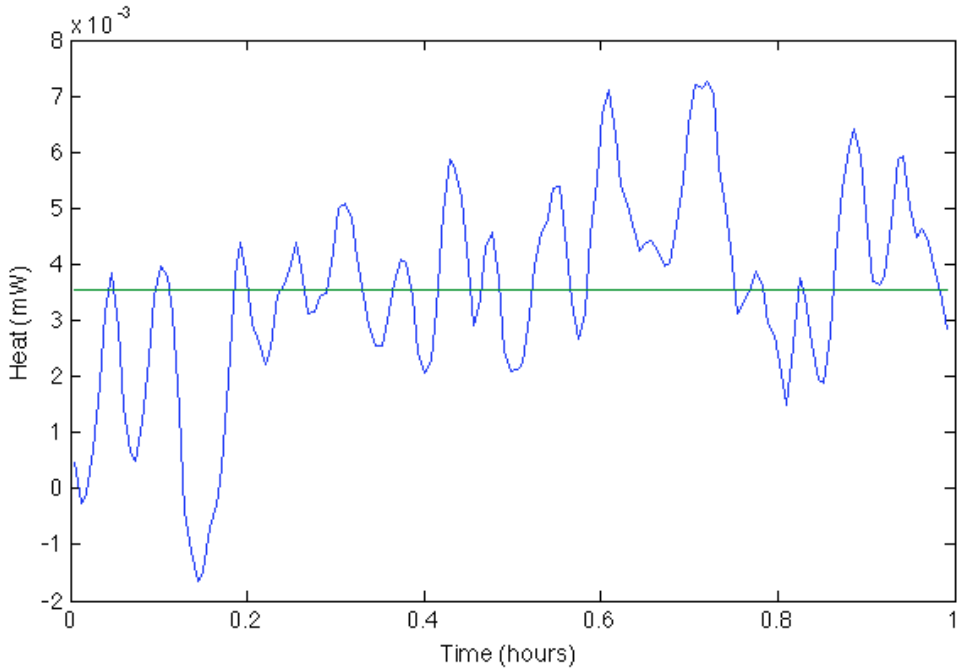

Figure 20: The heat during the one hour rest at the beginning of the test with the average shown in green

The noise experience by the heat during this 1 hour resting region (showed in Figure 20) is found to be inside a window of 0.008mW. During the constant voltage range of testing (area of interest), heat is found to be around 0.4mW, thus the error is around 2%.

Error in the heat due to dynamics was also analyzed by observing Figure 20 (See Section 4.6 for more details on how Figure 21 was developed). Figure 21 shows a comparison between theoretical heat generation (Q*) and heat generation data collected from the calorimeter (Q).

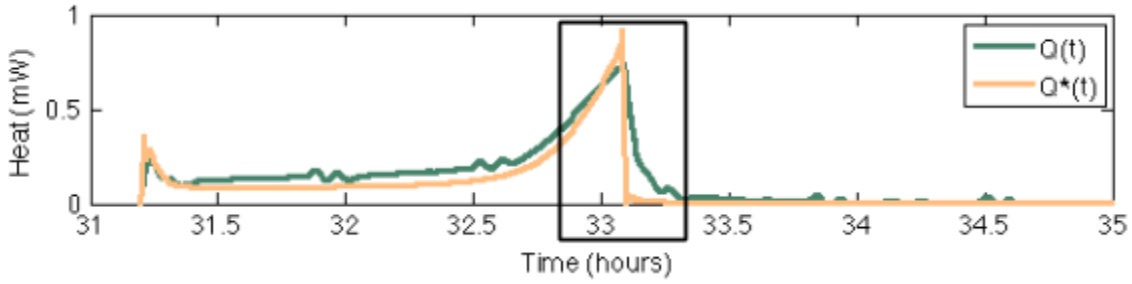

Figure 21: Emphasis on the time constant experienced by the calorimeter

It is important to note the boxed region showed in Figure 21. A time constant due to the thermal mass of the calorimeter causes an associated time lag in the heat measurements. This time constant can be determined by finding the additional time for the heat to reach zero (difference in time for Q* and Q to reach zero when current is removed). This time constant value was approximated to be 15-20 minutes. Since this study looks primarily at the non-dynamic, ohmic region of the test and that test last from 1-5 hours, it can be concluded that during this central region there will be an area where this time constant will not longer be prevalent.

4.6 Heat Generation Comparison for Different C-Rates

For this study, a comparison was performed for the test outlined in Section 4.4. A close up of the portion of interest (discharge and rest) can be seen in Figure 22.

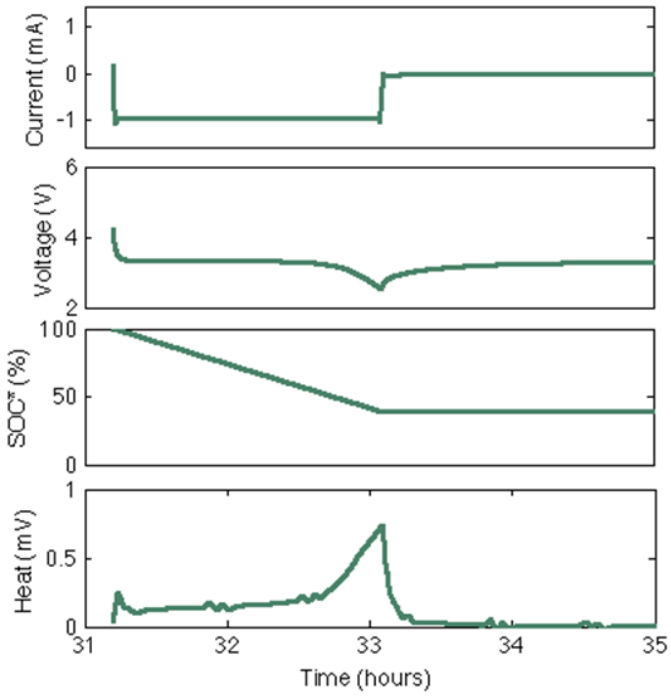

Figure 22: Close up of raw data for discharge and resting portion of test

As the discharging current is applied, the voltage of the cell experiences an initial drop the begins to exponentially level out to a constant voltage. This can be explained by observing the electrical model for a battery shown in Figure 23.

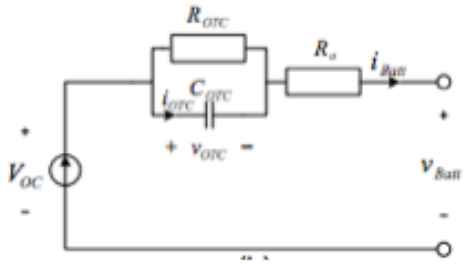

Figure 23: Electrical model of a battery

The initial drop can be explained by R_o and the exponential portion is due to the charging of capacitor C_{OTC}. When the capacitor is fully charged, R_o and R_{OTC} act as resistors in series, resulting in the constant voltage region. The exponential decrease

towards the end of the discharging process can be explained by a phenomena seen during the end of a discharging process when the last of the electrons in the cathode are pulled to the anode. During resting, it is observed that voltage then relaxes to the open circuit voltage. This is due to the charged capacitor C_{OTC} discharging.

To further verify the data, theoretical heat generation was compared to heat generation data collected from the calorimeter. Additional testing was used to get open circuit voltage data for each cell being compared. Open circuit voltage data was developed from charging and discharging the cell at C/20 from the minimum voltage of 2.5 volts to the maximum voltage of 4.2V. Using this data the capacity of the cell (C_{nom}) could be calculated for charging and discharging using Equation 16.

$$C_{nom} = \int_{V_{min}}^{V_{max}} Idt \qquad (16)$$

After the capacity of the cell was calculated, the state of charge (SOC) could be calculated for any test by using Equation 17.

$$SOC = SOC_o - \frac{1}{C_{nom}} \int Idt \qquad (17)$$

In Equation 17, SOC_o refers to the state of charge at the beginning of testing.

With SOC data, the C/20 data (also referred to as open circuit voltage data) could be plotted vs SOC. This plot could then be used as a reference for the open circuit voltage of any cell at any SOC. This is the plot needed need to apply Equation 18 and calculate the theoretical heat generation in a cell.

$$\dot{Q} = P_{ideal} - P_{actual} = I(V_{oc} - V) \qquad (18)$$

As seen in Equation 18, the theoretical heat generation is equal to the ideal

power produced by the power subtracted from the actual power produced by the battery, which is equivalent to the difference of the open circuit voltage and the actual voltage multiplied by the current at any point during charging or discharging of a batter. This method was used to calculate the theoretical heat generation during testing, Q*(t), and was compared to the heat generation data collected by the calorimeter, Q(t). The associated plots of this verification can be found in Figure 24.

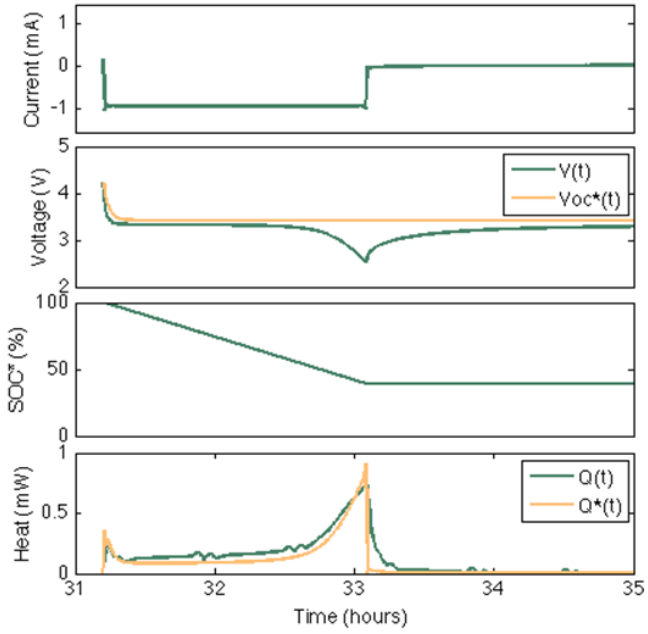

Figure 24: Verification of Calorimetry Heat Generation Data

As previously noted, the difference between the calculated heat generation and the actual heat generation seen at the end of discharge can be explained by the time constant of the calorimeter. Otherwise, the calculated and collected data are very similar, verifying the model.

After the data collected was verified with the theoretical heat generation model, testing at different C-Rates were compared. Figures 25 and 26 show the

comparison of voltage and heat generation during discharge of an aged cathode fabricated coin cell (C04).

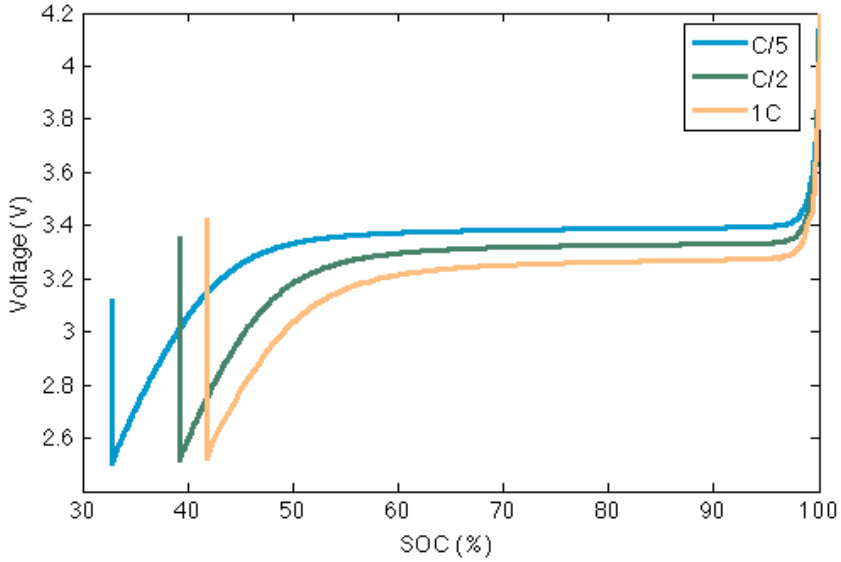

Figure 25: Voltage comparison of different C-Rates during discharge of C04 coin cell

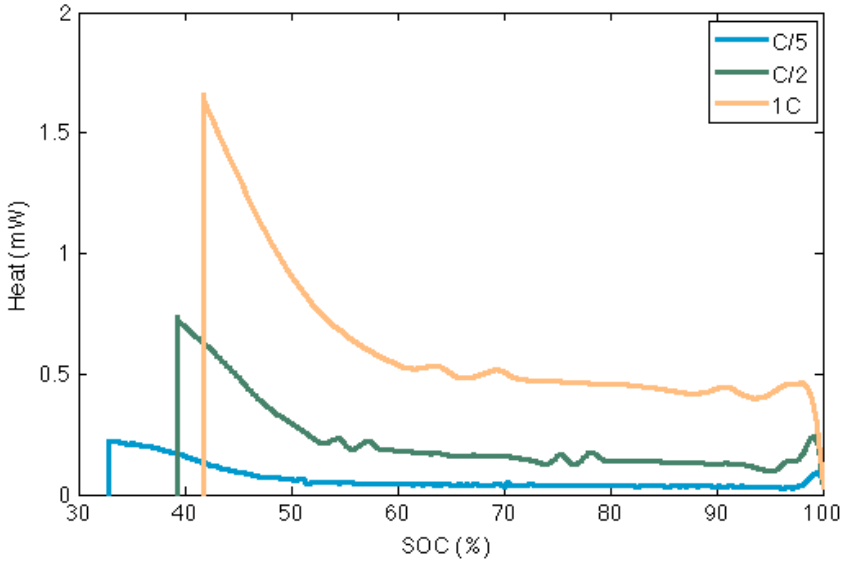

Figure 26: Heat generation comparison of different C-Rates during discharge of a C04 coin cell

Looking at Figure 25, it is important to note that each test ended at a different SOC. As

C-Rate increased, the minimum SOC increased. This coincides with common knowledge. Figure 26 also displays common trends. As C-Rate increases, the amount of heat generated increases in a similar manner. It is important to identify this in the constant voltage region where heat is mainly a function of current and internal resistance. As the beginning of the heat curve, a small peak is seen due to the activation energy used for the start of the discharge. In addition, the quadratic increase at the end of discharge is due to the additional energy used to remove the last electrons from the anode.

Is is also of interest to compare the efficiency for different C-Rates. Using a simple energy balance as seen in Figure 27, an equation for the efficiency during discharge can be derived (See Equations 19 and 20). The results of the efficiency comparison can be seen in Figure 27.

$$P_{chem} = P_{elec} + \dot{Q} \qquad (20)$$

$$\eta_{discharge} = \frac{P_{elec}}{P_{chem}} = \frac{P_{elec}}{P_{elec}+\dot{Q}} \qquad (21)$$

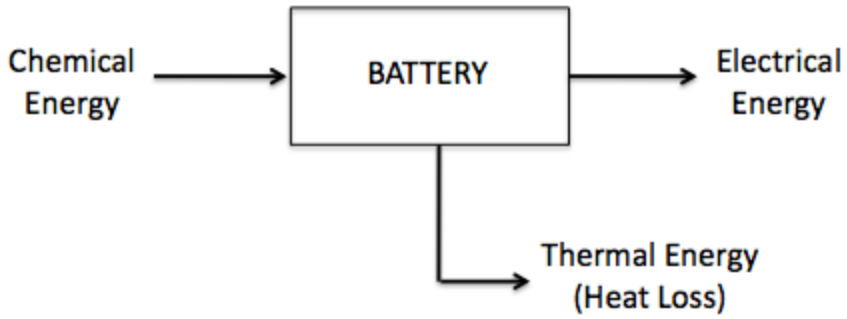

Figure 27: Energy balance of a battery for charging and discharging

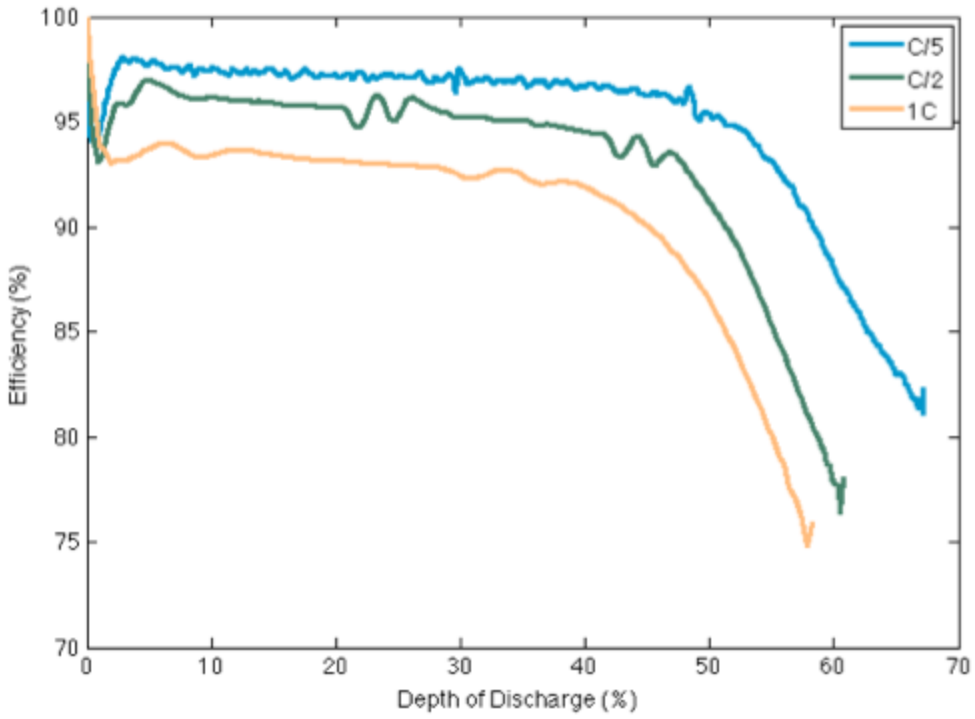

Figure 28: Efficiency during discharge of C04 coin cell for different C-Rates

The plot of efficiency during discharge for different C-Rates (Figure 28) displays similar trends to that of the heat generation plot (Figure 26) due to the direct relationship to heat. Overall, efficiency decreases with a corresponding increase in C-Rate, as expected.

It is also of interest to compare internal resistance for tests at different C-Rates. With Equation 21, internal resistance was calculated and plotted vs the depth of discharge as seen in Figure 29.

$$\dot{Q} = i^2 R \qquad (22)$$

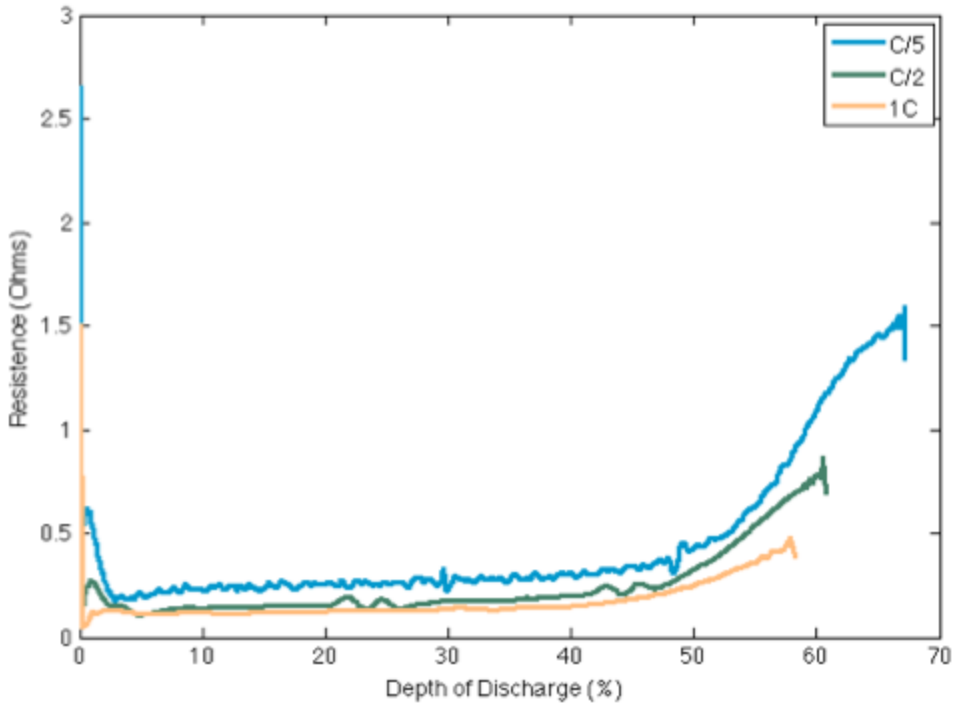

Figure 29: Efficiency during discharge of C04 coin cell for different C-Rates

As with the efficiency plot, it is essential to observe the central portion of the resistance plot (Figure 29) where the voltage during discharge remained primarily constant. During this region, internal resistance increased with decreasing C-Rate.

Overall, calorimetry data was able to be used to compare factors such as heat generation, efficiency, and internal resistance at different C-Rates. Data used was taken from discharging a C04 aged cathode fabricated coin cell at C/5, C/2, and 1C. The results coincided with expected trends.

4.7 Heat Generation Comparison for Aged and Non-Aged

In addition to comparing the data of a single cell at varying C-Rates, data taken with an aged C04 cathode coin cell was compared with data taken from an unaged C11 cathode coin cell. The analysis was performed with the same procedure as

described in Section 4.3.

Figures 30 and 31 show the comparison of heat generation for aged and unaged cells at discharging rates of C/5 and C/2.

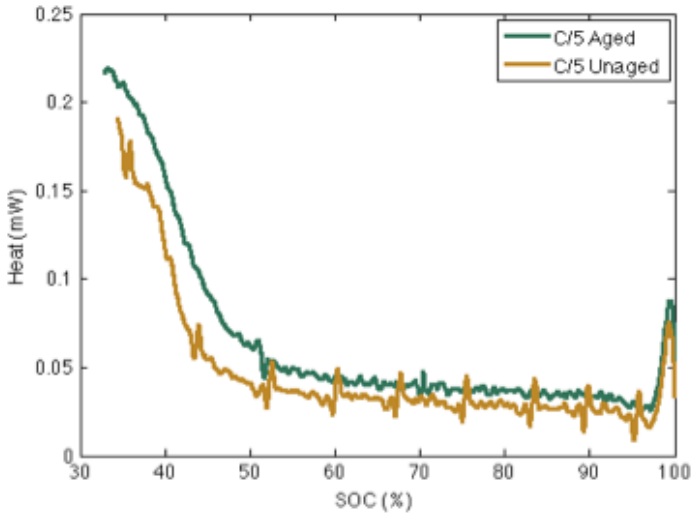

Figure 30: Comparison of heat generation for aged vs unaged cells at C/5

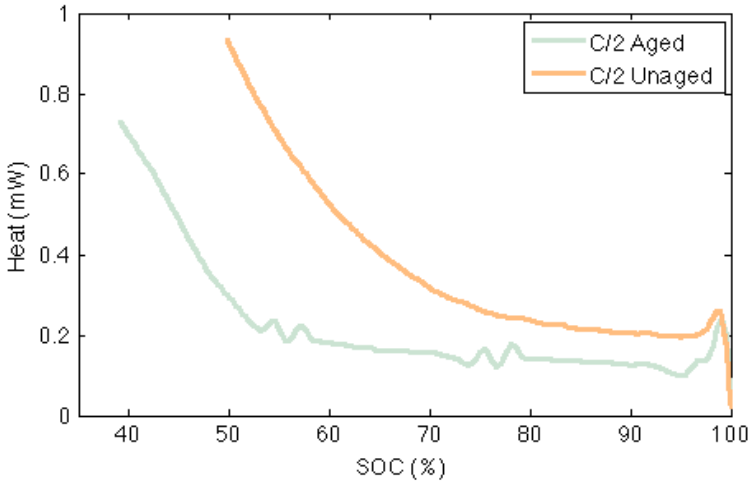

Figure 31: Comparison of heat generation for aged vs unaged cells at C/2

For the comparison at C/5 (Figure 30), it can be seen that both the aged and unaged cells exhibit primarily the same heat generation behavior. Looking at the

plots of C/2 (Figure 31), it can be seen that the unaged cell produced more heat than the aged cell. Figures 32 and 33 shows Internal Resistance and Efficiency calculated from the same data. These plots show similar trends. For the C/5 tests, aged and unaged cells displayed similar trends. For the tests at C/2, the unaged cell showed results that were less efficient and a higher internal resistance than the aged.

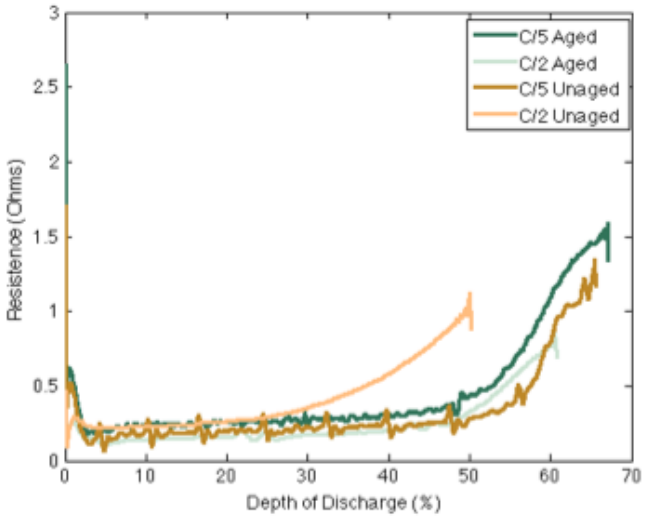

Figure 32: Comparison of Internal Resistance for Aged vs Unaged cells

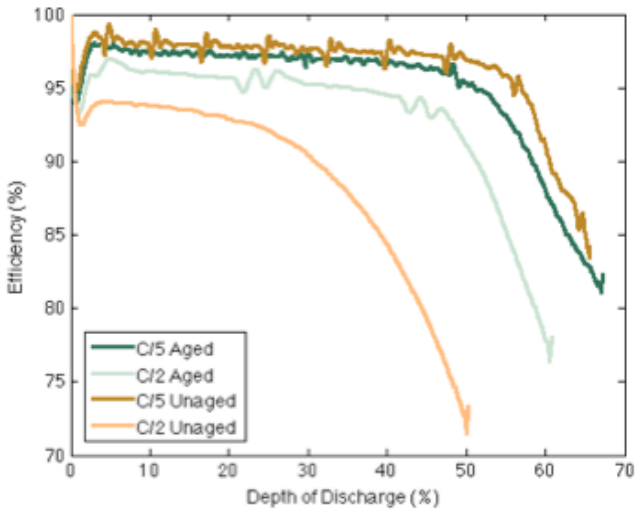

Figure 33: Comparison of Efficiency for Aged vs Unaged cells

These results tend to be contrary to typical behavior. It has been known that the aged cells should produce a greater amount of heat generation. With this known, tests were compared for two coin cells fabricated from the battery. Figure 34 shows the results of heat generation produced during discharging at C/5.

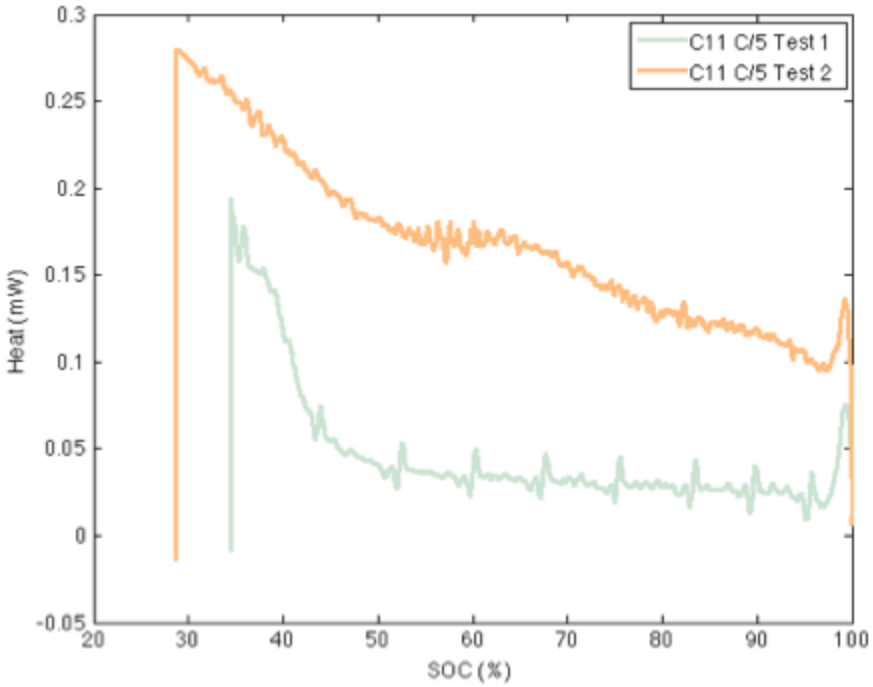

Figure 34: Heat generation of two cells fabricated from the same unaged battery

Looking at Figure 34, one can see that two cells fabricated the same type of battery still produce different heat generation profiles when tested at the same conditions. It is concluded that the reason for this could be the variations in fabricating the coin cells. It seems that the differences in producing this cells overcomes the differences between aged and unaged cells.

Chapter 5: Conclusion and Future Work

In conclusion, a methodology for testing thermal qualities of batteries using a calorimeter was established. Fabricated coin cells were tested using an Isothermal Battery Calorimeter in order to determine heat capacity, heat generation at different capacity rates, and heat generation for aged and unaged cells. Each of these tests were completed and results were able to be collected and analyzed. For the heat capacity tests, consistent results were determined, however, more testing will need to be performed in order to fully verify the testing procedure. For the capacity tests, factors such as heat generation, internal resistance, and efficiency were able to be compared for different C-Rates. Data was able to be used to verify battery models and the comparison at different C-Rates showed expected results. However, when comparing the capacity tests of aged to unaged coin cells inconsistent results were found. It was concluded that differences in fabrication of the coin cells played a larger impact on the heat generation then the differences found due to aging. Thus, for this methodology to be used to determine heat generation trends due to aging, an improved fabrication process in key.

References

[1] Jaclyn Trop and Bill Vlasic, "A Hankering for Hybrids," *The New York Times* (2013)

[2] Chris Woodyard, "'Motor Trend' Names Tesla Model S as Car of the Year," *USA Today* (2012)

[3] Electric Drive Transportation Association, "Electric drive vehicle sales figures (U.S. Market) - EV sales," http://www.electricdrive.org/, (2013)

[4] Yoshiyasu Saito, "Thermal Studies of A Lithium Ion Battery," *Journal of Power Sources* **68**, 451-454 (1997)

[5] T.Q. Duong, "*Challenges in Developing Batteries for PHEV Applications*," First International Conference on Advanced Lithium Batteries for Automobile Applications, Argonne National Laboratory, 2008.

[6] Said Al-Hallaj, "Thermal modeling of secondary lithium batteries for electric vehicle/hybrid electric vehicle applications," *Journal of Power Sources* **110**, 341-348 (2002)

[7] J. Vetter, "Ageing mechanisms in lithium-ion batteries," *Journal of Power Sources* **147**, 269-281 (2005)

[8] Bo Jiang, "From Electrode Materials to Dynamic Models of Li-ion Cells," *The Ohio State University, Undergraduate Honors Thesis,* (2013)

[9] Laidler, Keith, J. (1993). *The World of Physical Chemistry*. Oxford University Press.

[10] Princeton LDA. (2013). http://www.princeton.edu/~achaney/tmve/wiki100k/docs/Calorimeter.html

[11] *Thermal Hazard Technology.* (2013). http://www.thermalhazardtechnology.com/products/isothermal+battery+calorimeter+cc

[12] Ahmad A. Pesaran, "A Unique Calorimeter-Cycler for Evaluating High-Power Battery Modules," *IEEE,* 127-131 (1998)

[13] "Isothermal Battery Calorimeter-IBC Technical Application Note 1: Charge and discharge testing of two 18650 lithium-ion batteries," *Thermal Hazard Technology*

[14] C. Mi, A. Masrur, W. Gao, "Modern Hybrid Electric Vehicles," Wiley (2011)

[15] L. Guzzella, A. Sciarretta, "Vehicle Propulsion Systems," Springer (2005)

[16] F. Incropera, D. Dewitt, T. Bergman, “Introduction to Heat Transfer,” Wiley (2011)